Glycoconjugate Journal (1998) **15:** 309–321

EGC2
Solution conformation and dynamics of a fungal cell wall polysaccharide isolated from *Microsporum gypseum*

Ana Poveda[1], Manuel Martin-Pastor[3], Manuel Bernabe, Juan A. Leal[2], Jesus Jimenez-Barbero[3]*

[1] *Servicio Interdepartamental de Investigación, Universidad Autonoma de Madrid, Cantoblanco 28049 Madrid, Spain*
[2] *Centro de Investigaciones Biológicas, CSIC, Velazquez, 28006 Madrid, Spain*
[3] *Grupo de Carbohidratos, Instituto Quimica Organica, CSIC, Juan de la Cierva 3, 28006 Madrid, Spain*

The conformational and dynamical features of a branched mannan isolated from a fungal cell wall have been analysed by homo and heteronuclear NMR methods, employing different magnetic fields. ^{1}H NMR cross relaxation times have been obtained for this polysaccharide and have been interpreted qualitatively using different motional models. ^{13}C NMR relaxation parameters (T_1, T_2, NOE) have also been measured and interpreted using different approximations based on the Lipari and Szabo model free approach. The analysis of the data indicate the existence of important flexibility for the different linkages of the polysaccharide. Motions in the range of 4–6 ns contribute to the relaxation of the macromolecule, although faster internal motions in the 500 ps and 100 ps timescales are also present. These time scales indicate that segmental motions as well as internal motions around the glycosidic linkages are the major sources of relaxation for this molecule at 318 K. Molecular dynamics simulations have also been performed. The obtained results also indicate that the polysaccharide possess a substantial amount of conformational freedom.

***Keywords*: NMR spectroscopy, conformation, dynamics, relaxation**

Introduction

Mannans are constituents of many fungal cell walls, where they play a variety of biological and physiological functions, as protection of the cell wall, participation in cell–cell recognition and adherence of the microorganism to host cells [1]. These polysaccharides are present in dermatophytes, which are a variety of fungi which parasitize men and other mammals and which cause cutaneous infections mainly involving the keratinized tissues of nails, epidermis, and pilosebaceous follicles [2]. We have recently reported on the determination of the primary structure of a variety of polysaccharides isolated from several *Aphanoascus*, *Microsporum*, and *Trichophyton* [3]. Recently, a polysaccharide constituting a linear chain of $(1\rightarrow6)$-α-Manp-$(1\rightarrow6)$-α-Manp-$(1\rightarrow]_n$ entities, substituted every three residues at position two by an α-Manp-$(1\rightarrow2)$- moiety, was identified as the major component of the water soluble fraction of the cell wall of *Microsporum gypseum* [4]. This structure is particularly interesting from the conformational point of view, since both α-Manp-$(1\rightarrow2)$- and α-Manp-$(1\rightarrow6)$-linkages are present in the carbohydrate chains of glycoproteins [5]. The extent and nature of the motion around the glycosidic linkages of oligosaccharides remains an open question [6], and even detailed analysis of experimental and theoretical results have concluded either constrained conformations [7] or conformational averaging [8] for carbohydrate structures. The existence of rigid or flexible structures is of prime importance in recognition phenomena, since any bimolecular binding process is, in principle, entropically unfavourable due to the formation of a single complex molecule [9]. In addition, recent investigations have established that the rates of overall and internal motions of small and medium-size oligosaccharides may occur on similar timescales [10]. Thus, indication of internal motions around the glycosidic linkages of different disaccharides [11] and larger oligosaccharides has been obtained using both homo and heteronuclear NMR spectroscopy, as also employed for other biomolecules [12]. Experimental and theoretical reports have indicated that the α-Manp-$(1\rightarrow2)$-α-Manp glycosidic linkage is fairly rigid [13], while the α-Manp-$(1\rightarrow6)$-α-Manp linkage is rather flexible [14]. In this context, we

* To whom correspondence should be addressed.

0282–0080 © 1998 Chapman & Hall

decided to study the conformation and dynamic features of this polysaccharide [15], since, in principle, and due to its size, the time-scales of the overall tumbling and of the internal motions around the glycosidic linkages should be different and permit the analysis of the dynamical properties of the different glycosidic linkages. In addition, we have tried to characterize the extent of restriction to motion around the α-Manp-(1 → 6)-α-Manp linkage provided by the presence of the additional α-Manp-(1 → 2)- moiety [3]. Measurements of heteronuclear relaxation parameters for polysaccharides have allowed to probe variations in the relative motion of side chain versus backbone residues in branched polysaccharides [15, 16]. Nevertheless, a detailed and quantitative solution to the problem of polysaccharide dynamics is far from trivial and different models have been developed to describe the motion of these biomolecules. We now report on the application of NMR relaxation parameters, measured at different magnetic fields [17], to characterize the motional properties of the mannan. It seems necessary to consider that, for flexible polysaccharides, above a given molecular weight, it has been reported that relaxation parameters are independent of chain length, because of the dominant contribution of segmental motion to the spectral density function [18]. Our relaxation data have been interpreted by using the model-free approach proposed by Lipari and Szabo [19], since in principle, this approach is useful to characterize the molecular dynamics of flexible macromolecules such as the polysaccharide under consideration. In addition, different approximations of this model-free approach have been employed [20, 21] (see also experimental), in an attempt to obtain information on the reorientation correlation times, as well as on the local dynamics at the glycosidic linkages.

Materials and methods

Molecular mechanics and dynamics calculations

Molecular mechanics and dynamics calculations were performed using the CVFF force field [22] within the INSIGHT II/DISCOVER programs of BIOSYM technologies (San Diego, CA, USA). Eight independent geometries of a model pentasaccharide (with three α-(1 → 6) linkages and one α-(1 → 2) linkage) were built by combining the two more stable gauche-gauche (G) and gauche-trans (T) conformers of the mannose hydroxymethyl group [23] and subjected to extensive energy minimization with conjugate gradients. Thus, the following initial combinations were used: GGG, GGT, GTG, TGG, TTG, TGT, GTT, and TTT. The first letter refers to the orientation of the hydroxymethyl group of the A residue, the second one to that of the C moiety, and the third one to the D exocyclic group. The corresponding hydroxymethyl group of the B residue was set as gauche–gauche. Then, every final minimized structure was used as starting geometry for molecular dynamics (MD) simulations in vacuo at 300 K, with a dielectric constant of 80, and a time step of 1 fs. The equilibration period was 100 ps. After this period, structures were saved every 0.5 ps. The total simulation time was 1 ns for every run. Average distances between intra-residue and inter-residue proton pairs were calculated from the dynamics simulations. The complete 8*1 ns trajectories were considered.

NMR Spectroscopy

NMR experiments were recorded on Varian Unity 500 and Bruker AMX-300 spectrometers, using an approximately 30 mg/ml solution of the polysaccharide.

^{1}H NMR experiments

Selective inversion of the anomeric protons was performed using the DANTE-Z module during 60 ms. 1D-NOESY experiments were recorded using mixing times of 100, 200, 400, and 500 ms. ROESY experiments [24] used mixing times of 100, 200, 300, and 400 ms. The rf carrier frequency was set at δ 6.0 ppm, and the spin locking field was 2.5 KHz. T-ROESY experiments [25] were performed using mixing times of 100, 200, 300, and 400 ms. The rf carrier frequency was set at the centre of the spectrum and the spin locking field was 6 KHz. Under these experimental conditions, T-ROESY cross-relaxation rates are the mean average between the corresponding NOESY and ROESY analogues, although free from spurious Hartmann-Hahn effects [26]. The experiments were carried out at 318 K. Cross relaxation rates were obtained as previously described by extrapolation at zero mixing time [10, 27, 28]. Good linearity were observed up to 400 ms (NOESY) and 300 ms (ROESY). Estimated errors were smaller than 10%.

Effective correlation times for selected proton pairs were obtained from $\sigma_{NOESY}/\sigma_{ROESY}$ ratios, since they depend as on τ_c.

$$\sigma_{NOESY} = (k^2/10)\tau[6\,J(2\omega) - J(0)]$$

$$\sigma_{ROESY} = (k^2/10)\tau[2\,J(0) + 3\,J(\omega)],$$

then, after developing the spectral density functions, $J(n\omega)$, in function of the correlation time, τ, and of the spectrometer frequency, ω_0.

$$\sigma_{NOESY}/\sigma_{ROESY} = (5 + 22\omega_0^2\tau_c^2 + \omega_0^2\tau_c^2/(5 + 8\omega_0^4\tau_c^4) - 4\omega_0^2\tau_c^4),$$

which is a quadratic equation in τ_c, which can be easily solved.

Fitting of the homonuclear relaxation data

Different motional models were used to correlate the experimental ^{1}H-NMR measurements with the molecular dynamics results and to extract order parameters, S^2 (or S_f^2) and overall, τ_0, and internal motion, τ_e, (or effective, τ_{eff}) correlation times for the different atom pairs of the mannan. In this work, we considered the Lipari and Szabo model-free approach (for both proton and carbon data) [19] and different approximations thereof, as described by Lommerse *et al.* [20].

These approximations are:

Model I: Rigid isotropic motion, with one global correlation time.

$$J(\omega) = \frac{\tau_0}{1 + (\omega\tau_0)^2}$$

Model II: The spectral density function is modified by assuming different generalized order parameters (S_f^2) for every proton-proton pair. Thus, the global correlation time accounts for the slow motions of the molecule and S_f^2 for the fast internal motions around the glycosidic linkages and/or the monosaccharide rings (first term of the spectral density function within the model-free approach).

$$J(\omega) = S_f^2 \frac{\tau_0}{1 + (\omega\tau_0)^2}$$

Model III: If the S_f^2 order parameters were not available, it was possible to include fast internal motions by assuming different effective correlation times for every proton-pair.

$$J(\omega) = \frac{\tau_{eff}}{1 + (\omega\tau_{eff})^2}$$

Model IV: Both S_f^2 and effective correlation times were used for every proton pair.

$$J(\omega) = S_f^2 \frac{\tau_{eff}}{1 + (\omega\tau_{eff})^2}$$

Model V: The regular Lipari-Szabo model free approach, where τ_e represent a single effective time describing the internal motions.

$$J(\omega) = \frac{S^2\tau_0}{(1 + \omega^2\tau_0^2)} + \frac{(1 - S^2)\tau}{(1 + \omega^2\tau^2)}$$

$$\tau = \tau_0\tau_e/(\tau_0 + \tau_e)$$

A simplex algorithm was used for fitting the experimental data to the different models [29]. A target function Rw was defined which represents the deviation between the calculated relaxation data and the experimental, with Rw = 0 for an exact fit.

$$Rw = \sqrt{\sum_{i=1}^{n} \frac{(\sigma_{NOE_i}^{calc} - \sigma_{NOE_i}^{exp})^2 + (\sigma_{ROE_i}^{calc} - \sigma_{ROE_i}^{exp})^2 + (\sigma_{T\text{-}ROE_i}^{calc} - \sigma_{T\text{-}ROE_i}^{exp})^2}{(\sigma_{NOE_i}^{exp})^2 + (\sigma_{ROE_i}^{exp})^2 + (\sigma_{T\text{-}ROE_i}^{exp})^2}}$$

The subscript *i* represent data for a particular proton pair, and *n* is the total number of proton pairs with available experimental data.

The fit to the experimental data was done in independent runs, first, for the intra-residue proton pairs (since there are basically no errors in their corresponding average distances), and then, for the inter-residue proton pairs (optimizing the order parameters and/or correlation times obtained in the previous step). All the calculations were performed with in-house software which is available from the authors upon request. The experimental cross relaxation rates (from both 300 and 500 MHz NOESY, ROESY and T-ROESY experiments) were used as input, along with the average distances deduced from the eight 1 ns MD simulations. The program then estimated the effective (or overall, depending on the model) correlation times and S^2 (S_f^2) which produced the best fit to the experimental data, depending on the chosen motion model. Initial rational guesses of order parameters (between 0.3 and 0.8) and fast correlation times (between 10 and 250 ps) were used in the calculations in order to fit the data. Different calculations with either all the relaxation parameters, or leaving out just one set (NOESY, ROESY, T-ROESY) of cross relaxation rates were used. In these cases, the parameter not used in the fitting was employed as test of the goodness of fit, by comparison of the simulated experimental data (using the optimized motional parameters) with the experimental ones. Only the results of the best fit (smallest Rw), obtained by including all the experimental data, are given in the text.

^{13}C NMR experiments

^{13}C-NMR T_1 relaxation times were obtained by both the regular 1D-inversion recovery and the 2D-double INEPT based inverse detection methods [30] at 45 °C at both 7 and 11.8 T. At least six different relaxation delays were used in every experiment. Heteronuclear NOEs were obtained by comparing the intensities of the signals of two spectra acquired by the standard 1D-protocol [17]. T_2 transverse relaxation times were obtained by the CPMG pulse sequence [17]. In all cases, the given values were averaged among the different measurements performed. Estimated errors were in all cases smaller than 10%.

$$T_1^{-1} = (\Omega/20)[J(\omega_H - \omega_C) + 3J(\omega_C) + 6J(\omega_H + \omega_C)]$$

$$T_2^{-1} = (\Omega/20)[4J(0) + J(\omega_H - \omega_C) + 3J(\omega_C) + 6J(\omega_H) + 6J(\omega_H + \omega_C)]$$

$$\Omega = N\left(\frac{\gamma_C\gamma_H\delta}{r_{CH}^3}\right)^2$$

$$NOE = 1 + \frac{\gamma_H}{\gamma_C}\frac{6J(\omega_C + \omega_H) - J(\omega_C - \omega_H)}{J(\omega_C - \omega_H) + 3J(\omega_C) + 6J(\omega_C + \omega_H)}$$

Fitting of the heteronuclear relaxation data

The fitting to the rigid model or to any truncated Lipari-Szabo approach (Models I–IV) did not produce satisfactory results and, thus, these results are not discussed further. The following models were employed:

Model V: The regular isotropic Lipari-Szabo model free approach [19], where τ_e represent a single effective correlation time describing the internal motions.

$$J(\omega) = \frac{S^2\tau_0}{(1 + \omega^2\tau_0^2)} + \frac{(1 - S^2)\tau}{(1 + \omega^2\tau^2)}$$

$$\tau = \tau_0\tau_e/(\tau_0 + \tau_e)$$

Model VI. Extended isotropic Lipari-Szabo model free approach as described by Clore *et al.* [21]. Two different

internal motions were considered, characterized by fast, τ'_f, and slow, τ'_s, correlation times. Order parameters for the corresponding motions were also included in the analysis.

$$J(\omega) = \frac{S^2\tau_0}{1+(\omega\tau_0)^2} + \frac{(1-S_f^2)\tau'_f}{1+(\omega\tau'_f)^2} + \frac{(S_f^2-S^2)\tau'_s}{1+(\omega\tau'_s)^2}$$

$$S^2 = S_f^2 \cdot S_s^2$$

$$\tau'_i = \tau_i\tau_0/(\tau_0+\tau_i), \quad i = f, s$$

If τ_f is much smaller than τ_s, then the spectral density function simplifies to Model VII:

$$J(\omega) = \frac{S^2\tau_0}{1+(\omega\tau_0)^2} + \frac{(S_f^2-S^2)\tau'_s}{1+(\omega\tau'_s)^2}$$

$$S^2 = S_f^2 \cdot S_s^2$$

$$\tau'_s = \tau_s\tau_0/(\tau_0+\tau_s)$$

Model VIII. Using a symmetric top within the Lipari Szabo approach. In this case, for an anisotropically tumbling molecule, two correlation times were defined, $\tau_\perp$ and $\tau_{||}$, along the short and long axis of the proellipsoid [17, 19]. θ was the angle between the C–H relaxation vector and the symmetry axis.

$$J(\omega) = S^2 J_{anisot}(\omega) + (1-S^2)\frac{\tau}{1+(\omega\tau)^2}$$

$$\tau^{-1} = \tau_0^{-1} + \tau_e^{-1}$$

$$J_{anisot}(\omega) = \frac{0.25(3\cos^2\theta - 1)^2\tau_a}{1+(\omega\tau_s)^2} + \frac{(3\sin^2\theta\cos^2\theta)\tau_b}{1+(\omega\tau_b)^2} + \frac{0.75(\sin^4\theta)\tau_c}{1+(\omega\tau_c)^2}$$

where:

$$\tau_a = \tau_\perp$$
$$(1/\tau_b) = 5/(6\tau_\perp) + 1/(6\tau_{||})$$
$$(1/\tau_c) = 1/(3\tau_\perp) + 2/(3\tau_{||})$$

For the hetero-nuclear relaxation parameters, a similar target function, Rw, was also defined:

$$Rw = \sqrt{\sum_{i=1}^{n} \frac{(T1_i^{calc} - T1_i^{exp})^2 + (T2_i^{calc} - T2_i^{exp})^2 + (NOE_i^{calc} - NOE_i^{exp})^2}{(T1_i^{exp})^2 + (T2_i^{exp})^2 + (NOE_i^{exp})^2}}$$

with Rw = 0, for an exact fit. The subscript *i* represents data for a particular carbon atom, and *n* is the total number of carbons for which experimental data are available.

As stated above, either all the relaxation parameters or combinations of two of them (always at both magnetic fields) were used. The parameter which was not taken into account in the fitting procedure, was employed as a test of the goodness of fit approach. In all cases, for the different models, only the results of the best fit (smallest Rw), that include all the experimental data are given in the text.

An estimation of the errors in the motional parameters obtained within each optimization was accomplished by fixing the maximum precision of the Rw to 0.001 around the best fitting value, and then observing the range of variability of the motional parameters. The minimization of the target functions Rw (homo-nuclear and hetero-nuclear) in the different calculations was accomplished, in an iterative way, by using a simplex-based algorithm [29, 31]. Since different variables had to be optimized, a recursive method was adopted, starting from 1, 2, up to a maximum of 5 (model VIII) variables evaluated simultaneously. Different intervals of values of the variables were screened in order to find the global minimum. All the programs, which are written in Pascal, are available from the authors upon request.

Results and discussion

Molecular dynamics studies

Information on the accessible amount of conformational space was obtained through MD simulations [32, 33] of the mannan. In vacuo simulations with the DISCOVER-CVFF programme [22] were performed, since they provided satisfactory results in the study of the conformation of a variety of oligosaccharide molecules [34, 35]. Eight different starting conformations of one pentasaccharide model (Figure 1), composed of all the different glycosidic linkages of the polysaccharide was built and submitted to different 1 ns simulations (see Materials and Methods). Typical results are presented in Figure 2. For all linkages, it can be observed that the glycosidic torsion angles cover a defined part of the complete Φ/Ψ map, which is fairly independent of the rotamer present at the hydroxymethyl group. The glycosidic torsion angles Φ and Ψ show oscillations around -60 and 180 degrees, respectively as observed in Figure 2. These torsional oscillations are more pronounced around Ψ, as

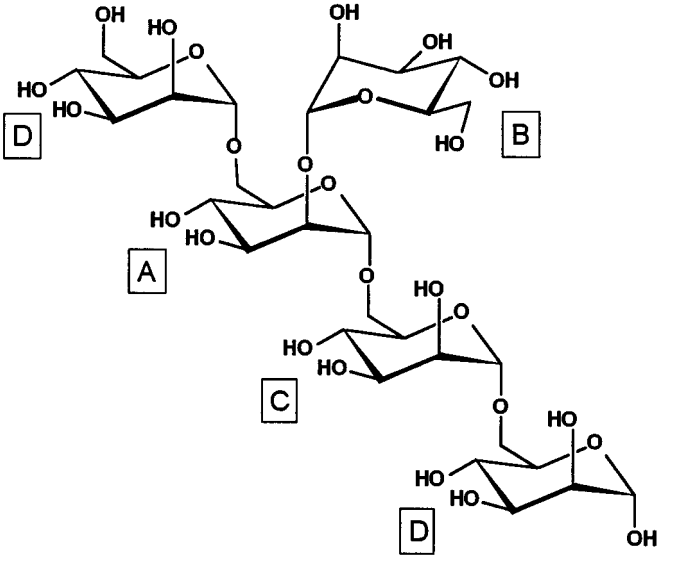

Figure 1. Schematic view of the polysaccharide chain, showing the different residues.

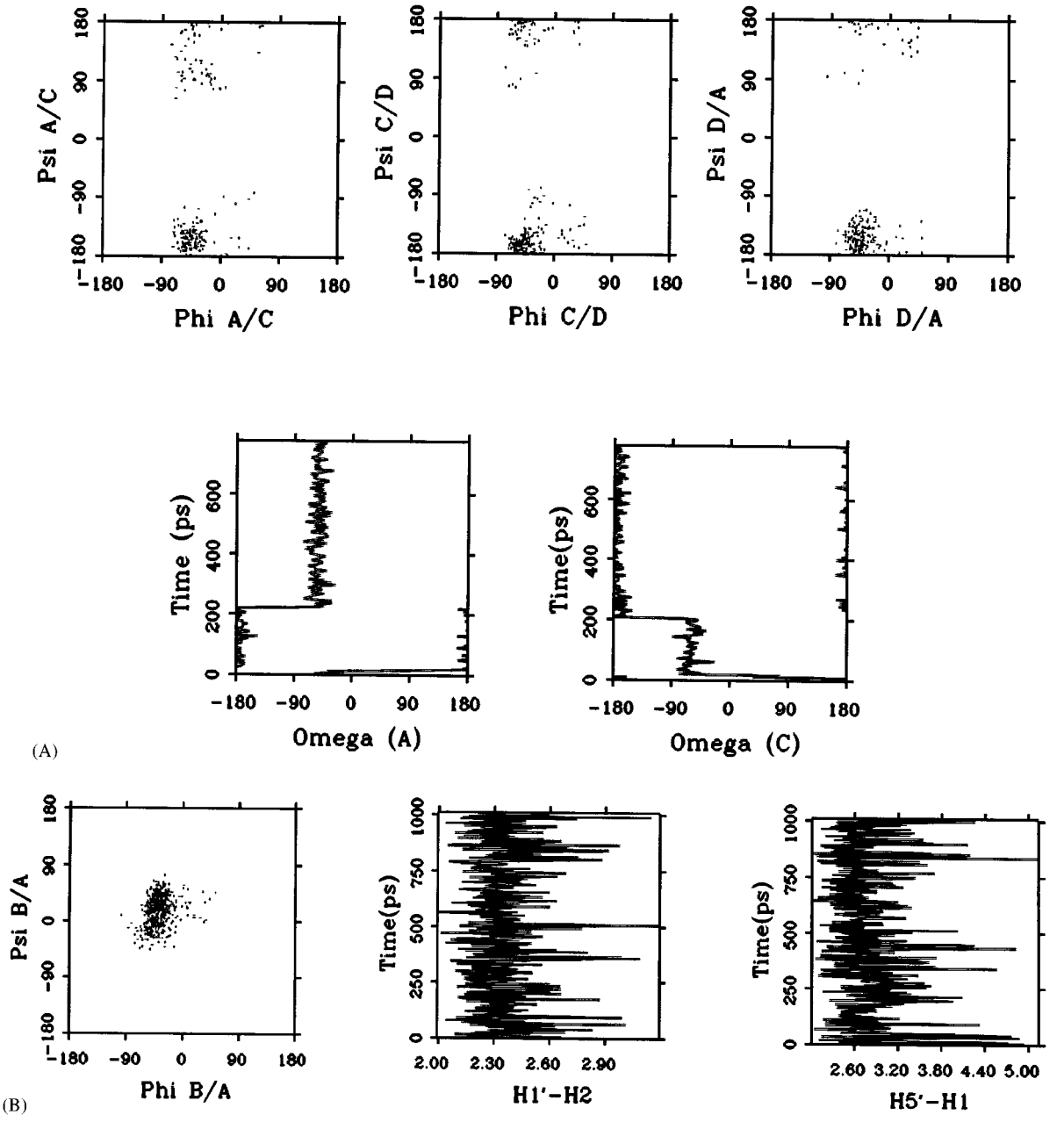

Figure 2. A) Instantaneous Φ/Ψ plots obtained for one of the MD trajectories, as calculated for a pentasaccharide fragment of the polysaccharide. The three top plots represent Φ/Ψ values for the three $1 \rightarrow 6$ linkages. From left to right A/C, C/D, and D/A, respectively. The two bottom plots show the trajectories obtained for the ω angles of residues A and C. The starting geometry was GTG. B) Instantaneous Φ/Ψ plot obtained for the $1 \rightarrow 2$ linkage during the same trajectory (left). The other two panels represent the variations of relevant inter- and intra-atomic distances found during the simulation.

expected by the operativity of the exo-anomeric effect around Φ [36]. As mentioned above, and explained in the experimental section, eight different 1 ns runs were performed with chosen starting geometries of the hydroxymethyl groups of the linear α-Manp-$(1 \rightarrow 6)$-main chain [23]. In terms of the available space for the interglycosidic torsion angles, the calculated results are fairly similar for the different α-$(1 \rightarrow 6)$- linkages, almost independent of the conformation (either *gg* or *gt*) of the lateral chain. With respect to the accessible conformational space for the α-Manp-$(1 \rightarrow 2)$-α-Manp linkage, the observed results (Figure 2B) are also independent of the conformation of the exocyclic chain at residues A and C, and are similar to those reported for the isolated disaccharide entity. In most cases, several transitions between the rotamers of the hydroxymethyl group were observed. Nevertheless, the hydroxymethyl groups displayed either the *gg* or the *gt* conformations for most of the simulation time (>90%,

[23]) Finally, average expected inter-proton distances (Figure 3) from the different MD simulations, Table 1) were used to generate expected inter-proton cross relaxation rates to be compared to those observed experimentally. This part has been discussed above. The obtained results may indicate that, as least for this particular case, these unrestrained MD simulations [37, 38] provide a fair description of the motion around the different glycosidic linkages of this molecule. A superimposition of different conformers found in the MD simulation is shown in Figure 4 and an extension of the pentasaccharide model to form a pentadecasaccharide is shown in Figure 5.

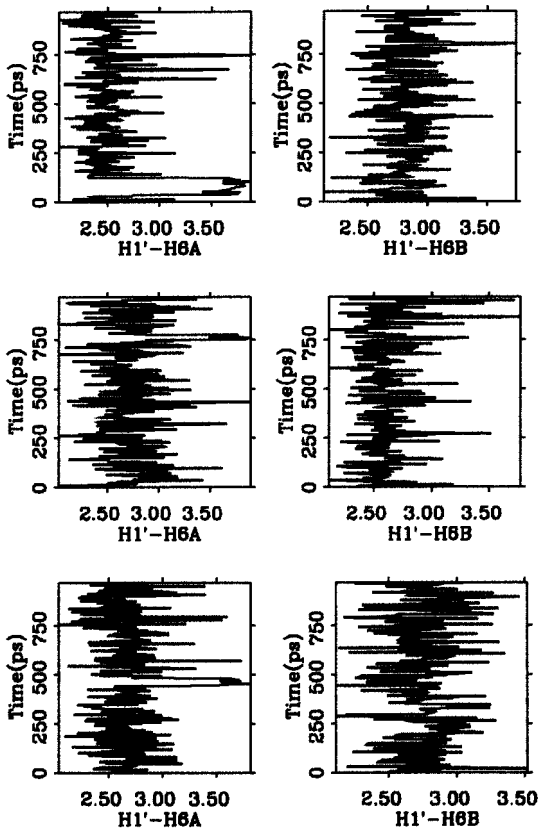

Figure 3. Variations of the relevant H-1′/H-6a and H-1′/H-6b interatomic distances found during the simulation which started with the GTG geometry. From top to bottom, the results for the A/C, C/D, and D/A glycosidic linkages are shown.

Table 1. Relevant inter-proton distances from different MD simulations using an average $\langle r^{-6} \rangle^{-1/6}$ value. The values are rounded.

Proton Pair	*Distance (Å)*
H-1 A/H-2 A	2.50
H-1 B/H-2 B	2.50
H-1 C/H-2 C	2.50
H-1 B/H-2 A	2.50
H-1 A/H-5 B	2.50
H-1 A/H-6a C	2.95
H-1 A/H-6b C	2.55
H-1 C/H-6a D	2.95
H-1 C/H-6b D	2.55

^{1}H-NMR Data

^{1}H-NMR cross relaxation rates [27] (σ_{ROE}, $\sigma_{T\text{-}ROE}$, and σ_{NOE}) were obtained from 1D-NOESY, 1D-ROESY, and 1D-TROESY (Figure 6) measurements, after selective

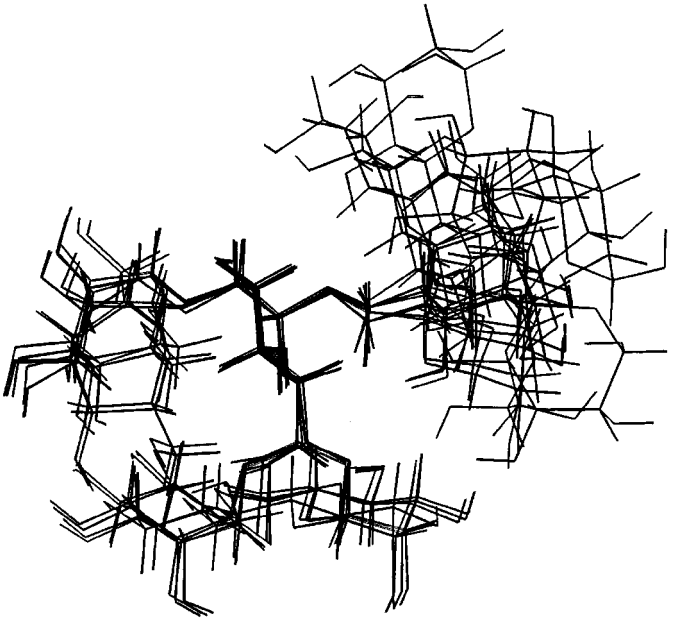

Figure 4. Superimposition of eight different snapshots taken from the *in vacuo* MD simulations performed for a pentasaccharide fragment of the polysaccharide. The existence of an important amount of flexibility around the $1 \rightarrow 6$ and $1 \rightarrow 2$ linkages is evident.

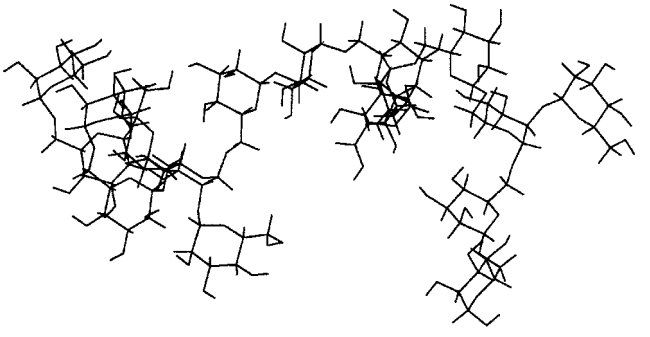

Figure 5. Structure of a possible pentadecasaccharide fragment of the polysaccharide, built from the different low energy regions for the glycosidic linkages.

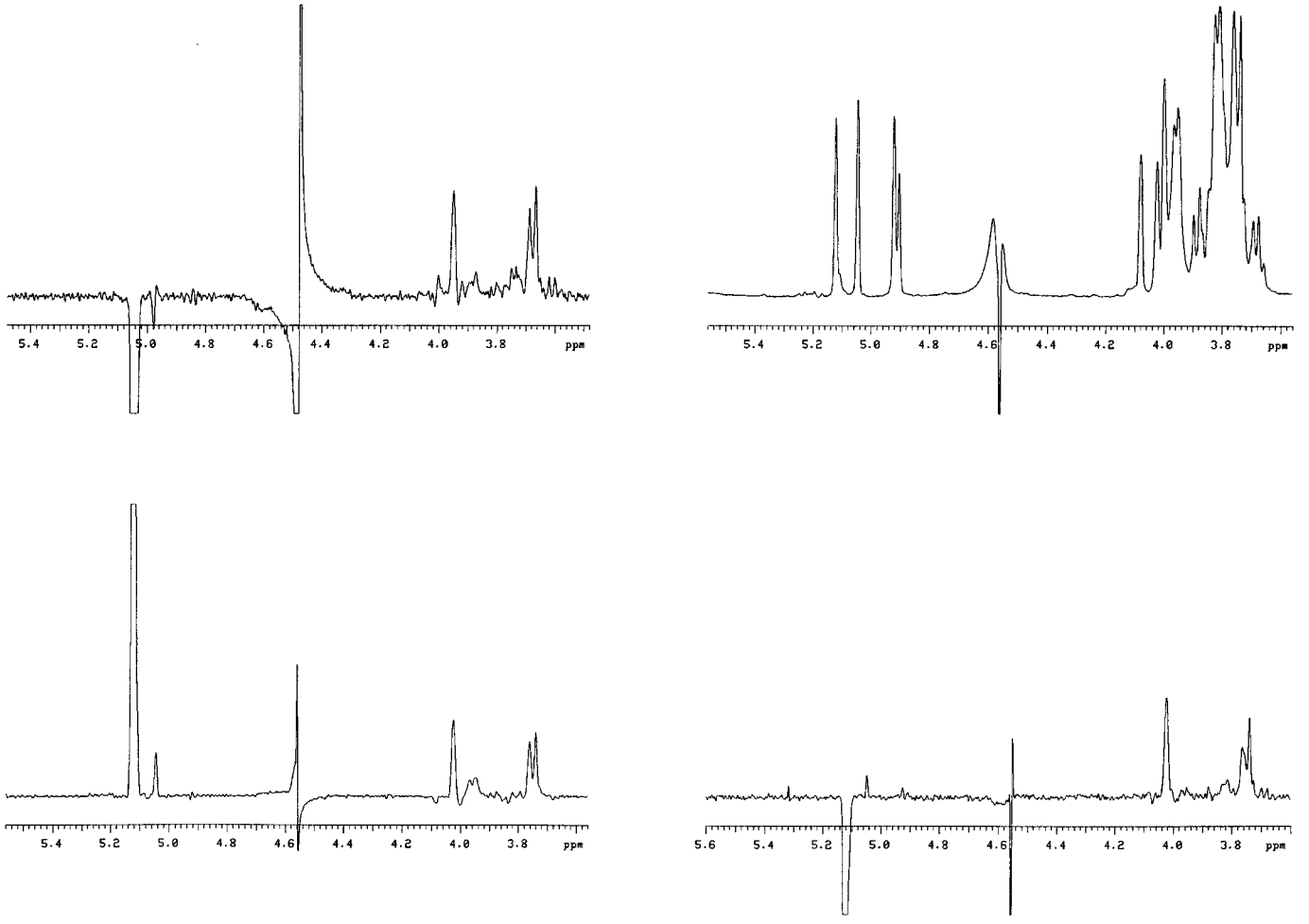

Figure 6. 1D-NOESY (bottom left), 1D-ROESY (bottom right), 1D-TROESY (top left) spectra obtained after inversion of the anomeric proton of residue A at 318 K. In all case, mixing time is 100 ms. The regular 1D spectrum is also shown (top right).

inversion of the anomeric protons (Table 2). 2D experiments were also performed. At 318 K, NOESY peaks are negative at both 300 and 500 MHz. A first attempt to characterize the presence of distinct internal motion for the different glycosidic linkages which constitute the polysaccharide was performed by obtaining $\sigma_{ROE}/\sigma_{NOE}$, $\sigma_{ROE}/\sigma_{T\text{-}ROE}$, and $\sigma_{T\text{-}ROE}/\sigma_{NOE}$ ratios at two magnetic fields [39, 40]. Provided that the motion was far from the extreme narrowing limit or the slow motion regimes, all these ratios were independent of inter-proton distances and allow to estimate specific correlation times (see methods). The results are also given in Table 2. It can be observed that, according to the ratios, and within experimental error, there were not relevant differences between intra- and inter-residue correlation times [10] ($\tau_c = 1.06 \pm 0.09$ ns) for the proton pairs of the different pyranoid rings, although the higher values were observed for residue A.

A somehow more quantitative approach was performed following a protocol similar to that described by Lommerse *et al.* [20]. Although the nature of the problem for polysaccharides is rather different to that existing in glycopeptides, we choose to test this protocol and, thus, effective correlation times were calculated from the simultaneous evaluation of all the proton cross relaxation data.

A fit of the experimental data to those calculated for the special density functions, $J(\omega)$, described by the isotropic model free approach of Lipari and Szabo (model V) and different approximations thereof (models I–IV) allowed us to estimate order parameters and internal motion correlation times. The analytical forms of these models have been given by Lommerse *et al.* [20], and are repeated in the Materials and Methods section of this paper for sake of clarity. Therefore, the explicit presence of flexibility around the different glycosidic linkages was considered in the analysis. The average interproton distances estimated according to a $(r^{-3})^{-1/3}$ averaging [27] (Table 1) from the MD simulations were used as input to calculate the theoretical NOESY, ROESY, and T-ROESY cross relaxation rates

Table 2. Experimental cross-relaxation rates (s^{-1}) for different proton pairs of the polysaccharide isolated from *M. Gypseum*; experimental error was smaller than 10%. Specific Correlation Times (ns) were estimated from the cross-relaxation rates ratios; estimated errors were ±10%.

Proton Pair	*NOESY 500 MHz*	*ROESY 500 MHz*	*T-ROESY 500 MHz*	*NOESY 300 MHz*	*T-ROESY 300 MHz*	*Correlation time (ns)*
H-1 A/H-2 A	− 0.180	0.650	0.190	− 0.145	0.175	1.15
H-1 B/H-2 B	− 0.140	0.595	0.175	− 0.120	0.190	1.02
H-1 C/H-2 C[a]	− 0.145	0.580	0.175	− 0.140	0.200	1.06
H-1 B/H-2 A	− 0.170	0.710	0.220	− 0.125	0.230	0.97
H-1 A/H-5 B	− 0.090	0.365	0.115	− 0.075	0.105	1.01
H-1 A/H-6a C	− 0.055	0.235	0.075	− 0.050	0.065	1.02
H-1 A/H-6b C	− 0.120	0.500	0.150	− 0.080	0.135	1.03
H-1 C/H-6a D[b]	− 0.050	0.215	0.075	− 0.045	0.055	1.00
H-1 C/H-6b D[b]	− 0.110	0.490	0.145	− 0.070	0.120	0.99

[a] Average values for H-1 C/H-2 C + H-1 D/H-2 D due to overlapping
[b] Average values for H-1 C/H-6 D and H-1 D/H-6 A due to overlapping

according to the different models [27, 41], at 300 and 500 MHz. Then, in the fitting protocol, order parameters and correlation times were varied in an iterative manner to match the experimental cross relaxation rates (Table 2). In a first step, only the four intra-residue H-1/H-2 rates were used for fitting. The estimated overall and/or effective τ_c and the internal correlation times, τ_e, are given in Table 3, along with the generalized order parameters S^2 (or S_f^2). As stated by Lommerse *et al.* [20], the estimations from the intra-residue proton pairs present a very minor dependence on conformation and may be correlated with the molecular dynamical features of the molecule. The largest variations of the local correlation times are found between residues A and B. These are not unexpected results, since A is the only substituted residue at the vicinity of the glycosidic linkage (at position 2), and residue B should experience both the motion around its own glycosidic linkage as well as additional fluctuations due to the motion of the main $(1 \rightarrow 6)$-chain [15, 16]. The goodness of fit was evaluated by using a residual factor, Rw [42]. The Rw values for the different models are also given in Table 3, which indicates that the best fit is obtained with the spectral density functions, $J(\omega)$ of the Lipari and Szabo model free approach [19]. Overall correlation times around 1–2 ns are obtained. The physical meaning of the obtained correlation times is not evident, since overall reorientation, segmental, internal motions of the pendant groups, and librations of the pyranoid rings are independent sources of modulation of dipole–dipole interactions [15, 43]. Nevertheless, the relatively small size of the obtained effective or overall correlation times by using these isotropic models (τ_c around 1–2 ns) indicated that local and segmental motions were the major sources of relaxation in this flexible polysaccharide [15, 18]. The obtained values of the relaxation parameters could correspond to those of the segment similar in size to the critical molecular weight or degree of polymerization for which relaxation parameters are independent of chain length [44]. In other flexible polysaccharide models, the minimum oligomer size for which segmental motion dominated the spectral power density was between 10 and 15 monosaccharide units [15, 18].

Table 3. Motional parameters for different intra-residue proton pairs of the polysaccharide of *M. Gypseum* obtained at 318 K from least squares fit of the experimental NOESY, ROESY, and T-ROESY cross relaxation rates. For models I, II and V, τ_{global} values correspond to τ_0 correlation time, for models III and IV they correspond to τ_{eff}. The residual factor Rw for models I and V was 0.271, 0.219, 0.224, 0.212 and 0.128 respectively.

Proton Pair	*Model*	τ_{global} *(ps)*	*Order Parameter*	τ_e *(ps)*
H-1/H-2 A	I	1002		
	II	1488	0.78	
	III	1193		
	IV	1660	0.78	
	V	1799	0.53	157
H-1/H-2 B	I	1002		
	II	1488	0.68	
	III	1032		
	IV	1369	0.67	
	V	1799	0.57	163
H-1/H-2 C	I	1002		
	II	1488	0.74	
	III	1080		
	IV	1310	0.75	
	V	1799	0.50	127
H-1/H-2 D	I	1002		
	II	1488	0.71	
	III	999		
	IV	1272	0.68	
	V	1799	0.54	121

Regarding the inter-residue cross-relaxation rates, these are obviously dependent on the three-dimensional conformation of the polysaccharide chain, that is, the torsional variations around Φ, Ψ and ω angles. Eight inter-residue proton cross-relaxation rates were analysed. The Rw values of the inter-residual pairs are given in Table 4 for each model. The best fit is again obtained for the model free approach, while the rigid isotropic model gives the worst one. It is evident that consideration of torsional flexibility by including local or effective correlation times and/or order parameters considerably improves the agreement between experimental and theoretical data. As stated above, the physical meaning of the correlation time is fairly ambiguous, and these values should be treated with caution. Nevertheless, with regard to the estimated order parameters, it is noteworthy to mention that the higher order parameters are always obtained for the A residue (the branching point of the polysaccharide). Similar order parameters (Table 4) were estimated for the non-substituted $(1 \rightarrow 6)$-linked moieties C and D. The smallest order parameter was observed for the $(1 \rightarrow 2)$-linked residue B. These values again indicate that B is affected by the motion of the main chain and by that of its own glycosidic linkage. Thus, similar observations to those indicated above for the local correlation times (Table 2) were observed. The results are in agreement with a higher individual restriction to motion of the $(1 \rightarrow 2)$ linkage in comparison to the $(1 \rightarrow 6)$ analogues. Order parameters for the intra-residue proton pairs are higher than those for the corresponding inter-residue analogues (Table 3). Therefore, and summarizing the results of the homonuclear experiments, the analysis of the experimental cross-relaxation data (Table 2), unequivocally indicate that there is an important amount of conformational freedom for the glycosidic and exocyclic torsion angles of this polysaccharide. Nevertheless, and at least qualitatively, it can be deduced that there are different extents of flexibility around the different glycosidic linkages. In addition, and according to the obtained τ_c values, segmental and local motions seem to be the major sources of dipole-dipole relaxation in the polysaccharide [15, 18]. Next, in order to try to characterize more profoundly the dynamic features of the polysaccharide, hetero-nuclear relaxation parameters were also measured.

Table 4. Motional parameters for different intraresidue proton pairs of the polysaccharide of *M. Gypseum* obtained at 318 K from least squares fitting of the experimental NOESY, ROESY, and T-ROESY cross relaxation rates. For models I, III and V τ_{global} values correspond to τ_0 correlation time, for models III and IV they correspond to τ_{eff}. The residual factor Rw for models I and V was 0.286, 0.223, 0.227, 0.215 and 0.161, respectively.

Proton Pair	*Model*	τ_{global} *(ps)*	*Order Parameter*	τ_e *(ps)*
H-1 A/H-5 B	I	971		
	II	1501	0.47	
	III	728		
	IV	973	0.67	
	V	2174	0.35	53
H-1 B/H-2 A	I	971		
	II	1501	0.79	
	III	1240		
	IV	1470	0.79	
	V	2174	0.53	235
H-1 A/H-6a C	I	971		
	II	1501	0.66	
	III	957		
	IV	1424	0.72	
	V	2174	0.47	102
H-1 A/H-6b C	I	971		
	II	1501	0.75	
	III	1100		
	IV	1433	0.77	
	V	2174	0.50	185
H-1 C/H-6a D[a]	I	971		
	II	1501	0.58	
	III	447		
	IV	1100	0.69	
	V	2174	0.39	68
H-1 C/H-6b D[a]	I	971		
	II	1501	0.64	
	III	936		
	IV	1254	0.75	
	V	2174	0.44	134

[a] Average values for H-1 C/H-6 D and H-1 D/H-6 A due to overlapping

^{13}C-NMR Data

Hetero-nuclear relaxation data are of paramount importance to detect the presence of internal motion in biomolecules, in general [45], and in carbohydrates, in particular [10, 11, 15, 46]. Regarding polysaccharides, relaxation parameters have been used either qualitatively or quantitatively to deduce their dynamical features [15–18]. Thus, in this case, T_1 and T_2 relaxation times and hetero-nuclear NOEs [45] were obtained, at two different magnetic fields, as described in the Methods section. Inspection of the average values (Table 5) of T_1 for the different residues of the mannan seem to indicate that residue B, thus, the α-Manp-$(1 \rightarrow 2)$-linked ring (with larger T_1 and NOEs), is less constrained than the α-Manp-$(1 \rightarrow 6)$- residues (smaller T_1 and NOEs). A similar trend has been previously observed in branched dextrans and, indeed, those values were used to assign the different anomeric carbon atoms of a series of polysaccharides in terms of branched, side-chain, and non-substituted residues [15–18]. The model-free approach was employed for the analysis of the relaxation data, since, in principle, it is adequate for flexible macromolecules. First, a isotropic model was employed. The Lipari and Szabo analysis [10, 17, 19, 41] of the hetero-nuclear data (Table 6)

Table 5. Longitudinal relaxation times (s), hetero-nuclear NOEs and transversal relaxation times (s) for the mannan at 75 and 125 MHz and 318 K, experimental errors are smaller than 10%.

Carbon Atom	*T1 75 MHz*	*T1 125 MHz*	*NOE 75 MHz*	*NOE 125 MHz*	*T2 75 MHz*	*T2 125 MHz*
C1-A	0.17	0.31	1.76	1.57	0.07	0.08
C2-A	0.18	0.33	1.59	1.44	0.10	0.11
C3-A	0.16	0.32	1.66	1.52	0.08	0.10
C4-A	0.19	0.29	1.70	1.46	0.08	0.10
C5-A	0.18	0.30	1.81	1.53	0.07	0.10
Average	0.18	0.31	1.68	1.50	0.08	0.10
C1-B	0.28	0.43	1.95	1.80	0.17	0.30
C2-B	0.25	0.37	1.88	1.64	0.11	0.10
C3-B	0.24	0.39	1.98	1.78	0.15	0.20
C4-B	0.24	0.35	1.98	1.71	0.15	0.20
C5-B	0.24	0.35	1.94	1.76	0.16	0.20
Average	0.25	0.38	1.84	1.74	0.15	0.20
C1-C	0.18	0.34	1.74	1.52	0.07	0.08
C2-C	0.24	0.35	1.88	1.64	0.11	0.15
C3-C	0.24	0.38	1.98	1.78	–	0.10
C4-C	0.24	0.32	1.71	1.56	0.04	0.05
C5-C	0.24	0.34	1.84	1.62	0.07	0.09
Average	0.23	0.35	1.80	1.63	0.07	0.09
C1-D	0.18	0.34	1.74	1.52	0.06	0.08
C2-D	0.24	0.36	1.88	1.64	0.11	0.15
C3-D	0.24	0.38	1.98	1.78	–	0.10
C4-D	0.24	0.32	1.71	1.56	0.04	0.05
C5-D	0.19	0.33	1.77	1.57	0.06	0.07
Average	0.22	0.34	1.78	1.60	0.07	0.09
C-6A	0.09	0.20	1.95	1.54	0.06	0.07
C-6B	0.12	0.23	1.99	1.87	0.10	0.13
C-6C	0.10	0.17	1.71	1.54	0.03	0.13
C-6D	0.08	0.16	1.77	1.49	0.06	0.06

Table 6. Average motional parameters of the different residues from ^{13}C NMR relaxation data for the methine groups of the mannan using Model V, $\tau_0 = 1005 \pm 50$ ps, $R_w = 0.054$.

Residue	τ_e *(ps)*	S^2	*Residue*	τ_e *(ps)*	S^2
A	159	0.80	C	172	0.67
B	110	0.49	D	169	0.69

estimated an overall correlation time of *ca.* 1 ns, with short local correlation times, τ_e, smaller than 250 ps for all the glycosidic linkages. The τ_e values were fairly similar to those obtained from the homonuclear data. S^2 values for the methine carbons were between 0.40 and 0.87, the smallest values being for the Manp-(1 → 2) B moiety (range 0.40–0.58) and the highest for the 2-O-substituted-α-Manp-(1 → 6) A residue (range 0.76–0.87). The values for the other residues (C and D) were in-between. As deduced from the homonuclear proton data, the sizes obtained for the overall correlation times (around 1 ns) indicated that local and segmental motions were the major sources of relaxation of this polysaccharide [15, 44]. The motional behaviour of the molecule, indicated that the relaxation data for this flexible macromolecule corresponded to an oligosaccharide segment of about 10–15 monosaccharide units [18].

Nevertheless, this isotropic analysis did not match the T_2 values in a satisfactory way, since the expected values were significantly higher than those experimentally measured [15, 17]. Thus, in a second step, and considering that it is certainly possible that different motions (time-scales) contribute to the observed relaxation parameters, an extended Lipari-Szabo model was applied, as proposed by Clore and coworkers [21] (see Materials and Methods). In this model, apart from the overall motion, two different internal motion correlation times and order parameters were considered, accounting for the existence of very fast (τ_f) and moderately

Table 7. Average motional parameters of the different residues from ^{13}C NMR relaxation data for the methine groups of the mannan using Model VI, $\tau_0 = 6430 \pm 300$ ps, $R_w = 0.012$.

Residue	τ_s' *(ps)*	τ_f' *(ps)*	S_s^2	S_f^2	*Residue*	τ_s' *(ps)*	τ_f' *(ps)*	S_s^2	S_f^2
A	835	80	0.31	0.87	C	617	70	0.39	0.83
B	754	57	0.14	0.55	D	616	83	0.4	0.85

fast (τ_s) internal motions. If τ_f is at least one order of magnitude smaller than τ_s, a truncated form may be considered (see Materials and Methods section). Thus, both non-truncated and truncated forms (models VI and VII, respectively) were considered, since the time-scales of the internal motions were not known *a priori*. Both models (Tables 7 and 8) provided a fairly satisfactory matching between expected and observed data (fairly small Rw). The overall correlation times were between 6.5 and 4.0 ns respectively, depending on whether an extended or truncated model was considered. The slow internal motions were between 500 (truncated model) and 700 ps (extended model). Finally, the very fast internal motions (model VI) were around 100 ps. Regarding order parameters, the branched A rings presented the largest restriction to motion, while the B side chain units showed the smallest S^2. The order parameters for C and D rings were in-between. With regard to the different motions [15–18], it seemed that the obtained overall correlation times (*ca.* 4–6 ns) corresponded to the segmental motion timescale, while the fast correlation times probably included the motion around the ω torsions, around the Φ/Ψ glycosidic linkages, and the freeing of the pyranoid rings [43]. Probably, the time-scale around 500 ps included the first two types of motions, while the fast correlation times obtained around 100 ps were contributions of the last two types [15–18].

Finally, in order to explore the possibility of the existence of anisotropic motion, the polysaccharide was considered as a symmetric top molecule [17], characterized by two different overall correlation times, $\tau_\perp$ and $\tau_{||}$, and a term that included a local motion correlation time, τ. Although the use of any model for a polysaccharide is a matter of discussion [15–18], fitting the data showed that the existence of a proellipsoid shape could be possible. In fact, there was again a satisfactory matching between all the experimental and expected relaxation data (Table 9). The ratio between $\tau_\perp/\tau_{||}$ was about 18, $\tau_{||}$ being around 0.5 ns. The internal motion correlation times were *ca.* 100 ps. This anisotropic analysis of the data also allowed us to conclude, (also concluded after assuming isotropic motion) that the outer ring displayed rather significant local motion, characterized by the lower order parameters for all of its carbons.

Thus, independent of the model used, and as also deduced from the ^{1}H NMR relaxation data, the above conclusion indicated that the relaxation of the B ring atoms was modulated by the motion of the linear chain, as well as by that existing around its glycosidic linkage. For the rings of the α-(1 → 6) linear chain, the data again indicated the existence of a higher restriction to fast motions for the branched Manp residue. From these data there is a significant and measurable difference between the flexibility of the branched (A) and the non branched Manp-(1 → 6) (C, D moieties).

Table 8. Average motional parameters of the different residues from ^{13}C NMR relaxation data for the methine groups of the mannan using Model VII, $\tau_0 = 4165 \pm 400$ ps, $R_w = 0.022$.

Residue	τ_s' *(ps)*	S_s^2	S_f^2	*Residue*	τ_s' *(ps)*	S_s^2	S_f^2
A	576	0.45	0.97	C	473	0.41	0.88
B	453	0.29	0.72	D	475	0.42	0.89

Table 9. Average motional parameters of the different residues from ^{13}C NMR relaxation data for the methine groups of the mannan using Model VIII, $\tau_\perp = 8000 \pm 1500$ ps, $\tau_{||} = 439 \pm 25$ ps, $R_w = 0.027$.

Residue	θ	τ *(ps)*	S^2	*Residue*	θ	τ *(ps)*	S^2
A	70	40	0.87	C	77	46	0.75
B	75	59	0.56	D	77	48	0.76

Additional information on the existence of different motional freedom for the different Manp residues came for the relaxation parameters measured for the exocyclic C-6 carbons. The fit of the relaxation data to the different models (Table 10) showed a higher restriction to motions for the hydroxymethyl group of residue C than for those present in the other α-Manp-(1 → 6) linkages. The exocyclic carbon of the α-Manp-(1 → 2) B moiety is the most flexible, independently of the model employed. According to the data discussed above, these are not unexpected results since the hydroxymethyl groups of residues C are those linked to the branching points of the polysaccharide.

In conclusion, we have obtained homo- and hetero-nuclear relaxation parameters for a fungal cell wall polysaccharide, which have been interpreted at different levels of complexity. The homo-nuclear relaxation data have provided qualitative evidence of the importance of internal and segmental motions in this polysaccharide. Hetero-nuclear

Table 10. Average motional parameters of the different residues from ^{13}C NMR relaxation data for the methylene groups of the mannan using Models V to VIII, τ_f' corresponds to τ in model VIII and to τ_e in model V, S_f^2 corresponds to S^2 in models V and VIII.

Model	*Carbon Atom*	*θ*	τ_s' *(ps)*	τ_f' *(ps)*	S_s^2	S_f^2
V	C-6A			240		0.67
	C-6B			79		0.36
	C-6C			90		0.80
	C-6D			248		0.72
VI	C-6A		637	1	0.13	0.70
	C-6B		827	57	0.13	0.38
	C-6C		722	65	0.43	0.83
	C-6D		759	19	0.20	0.80
VII	C-6A		629		0.11	0.73
	C-6B		336		0.36	0.64
	C-6C		514		0.49	0.88
	C-6D		663		0.27	0.84
VIII	C-6A	90		15		0.69
	C-6B	75		53		0.41
	C-6C	69		42		0.83
	C-6D	77		2		0.75

parameters have permitted us to detect that motions in the 4–6 ns time-scale, as well as others in the hundreds of ps timescales, are able to produce dipole-dipole relaxation in this polysaccharide. The nature of these motions are probably related to segmental motion and to reorientation around the hydroxymethyl and glycosidic torsion angles, respectively. Finally, internal motions faster than 100 ps are also present. These motions are probably also involved in reorientations around the glycosidic torsion angles and freeing of the pyranoid rings. Both the extended Lipari/Szabo approach, as proposed by Clore *et al.* [21] and an anisotropic symmetric top model provide a satisfactory agreement between expected and observed data. Giving the flexibility of the polysaccharide, the first model seems to be more realistic.

Acknowledgements

Financial support of DGICYT (project PB93-0172) is gratefully acknowledged. We thank Prof. Martín-Lomas for his interest and the SIdI-UAM for the facilities provided throughout this work.

References

1 Bishop CT, Perry MB, Blank F (1966) *Can J Chem* **44**: 2291–7.
2 Takeda T, Kawarasaki I, Ogihara Y (1981) *Carbohydr Res* **89**: 301–8.
3 Jimenez-Barbero J, Bernabe M, Leal JA, Prieto A, Gomez-Miranda B (1993) *Carbohydr Res* **250**: 289–99.
4 Jimenez-Barbero J, Prieto A, Gomez-Miranda B, Leal JA, Bernabe M (1995) *Carbohydr Res* **272**: 121–28.
5 a) Dwek RA (1995) *Science* **269**: 1234–5. b) Wyss DF, Choi JS, Wagner G (1995) *Biochemistry* **34**: 1622–34.
6 a) Hricovini M, Shah RN, Carver JP (1992) *Biochemistry* **31**: 10018–23. b) Rutherford TJ, Partridge J, Weller CT, Homans SW (1993) *Biochemistry* **32**: 12715–24. c) Bush CA (1992) *Curr Opin Struct Biol* **2**: 655–63. d) Rice KG, Wu P, Brand L, Lee YC (1993) *Curr Opin Struct Biol* **3**: 669–74. e) van Halbeek H (1994) *Curr Opin Struct Biol* **4**: 697–709.
7 a) Mukhopadhyay C, Miller KE, Bush CA (1994) *Biopolymers* **34**: 21–29. b) Rutherford TJ, Spackman DG, Simpson PJ, Homans SW (1994) *Glycobiology* **4**: 59–68. c) Lemieux RU (1989) *Chem Soc Rev* **18**: 347–74. d) Bock K (1983) *Pure Appl Chem* **55**: 605–22.
8 a) Carver JP (1993) *Pure Appl Chem* **65**: 763–70. b) Ejchart A, Dabrowski J, von der Lieth C-W (1992) *Magn Res Chem Soc Rev* **30**: S105–S114. c) Peters T, Weimar T (1994) *J Biomol NMR* **4**: 97–116.
9 Searle MS, Williams DH (1992) *J Am Chem Soc* **114**: 10690–97.
10 a) Poppe L, van Halbeek H (1992) *J Am Chem Soc* **114**: 1092–94. b) Hricovini M, Torri G (1995) *Carbohydr Res* **268**: 159–75. c) Hardy BJ, Egan W, Widmalm G (1995) *Int J Biol Macromol* **17–18**: 149–60.
11 a) Meyer C, Perez S, Herve du Penhoat C, Michon V (1993) *J Am Chem Soc* **115**: 10300–310. b) Braccini I, Michon V, Herve du Penhoat C, Imberty A, Perez S (1993) *Int J Biol Macromol* **15**: 52–55. c) Poveda A, Asensio JL, Martin-Pastor M, Jimenez-Barbero J (1996) *Chem Comm* :421–422. d) Bagley S, Kovacs H, Kowalewski J, Widmalm G (1992) *Magn Reson Chem* **30**: 733–739. e) Maler L, Lang J, Widmalm G, Kowalewski J (1995) *Magn Reson Chem* **33**: 541–48. f) Espinosa JF, Asensio JL, Bruix M, Jimenez-Barbero J (1996), *An Quim Int Ed* **96**: 320–4.
12 a) Bruschweiler R, Roux B, Blackledge M, Griesinger C, Karplus M, Ernst RR (1992) *J Am Chem Soc* **114**: 2289–302. b) Philippopoulos M, Lim C (1994) *J Phys Chem* **98**: 8264–73. c) Abseher R, Ludemann S, Schreiber H, Steinhauser O (1994) *J Am Chem Soc* **116**: 4006–18.
13 Edge CJ, Singh UC, Bazzo R, Taylor GL, Dwek RA, Rademacher TW (1990) *Biochemistry* **29**: 1971–74.
14 Cumming DA, Carver JP (1987) *Biochemistry* **26**: 6664–76.
15 Dais P (1995) *Adv Carbohydr Chem Biochem* **51**: 63–161.
16 Seymour FR, Knapp RD (1980) *Carbohydr Res* **81**: 67–103.
17 a) Kowalewski J, Widmalm G (1994) *J Phys Chem* **98**: 28–34. b) Hricovini M, Guerrini M, Torri G, Piani S, Ungarelli F (1995) *Carbohydr Res* **277**: 11–23. c) Maler L, Widmalm G, Kowalewski J (1996) *J Biomol NMR* **7**: 1–7. d) Roy R, Tropper D, Williams AJ, Brisson JR (1993) *Can J Chem* **71**: 1995–2006.
18 a) Benesi AJ, Brant DA (1985) *Macromolecules* **18**: 1109–16. b) Brant DA, Liu HS, Zhu ZS (1995) *Carbohydr Res* **278**: 11–26.
19 Lipari G, Szabo A (1982) *J Am Chem Soc* **104**: 4546–59.
20 Lommerse JPM, Kroon-Batenburg LMJ, Kron J, Kamerling JP, Vliegenthart JFG (1995) *J Biomol NMR* **5**: 79–94.
21 Clore GM, Driscoll PC, Wingfield PT, Gronenborn AM (1990) *J Am Chem Soc* **29**: 7387–400.
22 Hagler AT, Lifson S, Dauber P (1979) *J Am Chem Soc* **101**: 5122–30.

23 Bock K, Duus J (1994) *J Carbohydr Chem* **13**: 513–43.
24 Bothner-By AA, Stephens RL, Lee JM, Warren CD, Jeanloz RW (1984) *J Am Chem Soc* **106**: 811–13.
25 Hwang TL, Shaka AJ (1992) *J Am Chem Soc* **114**: 3157–59.
26 Bax A, Davis DG (1985) *J Magn Res* **63**: 207–13.
27 Neuhaus D, Williamson MP (1989) The Nuclear Overhauser effect in structural and conformational analysis, New York, VCH.
28 Esposito G, Pastore A (1988) *J Magn Res* **76**: 331–36, and references therein.
29 Craik DJ, Kumar A, Levy GC J (1983) *Chem Inf Comput Chem* **23**: 30–38.
30 Barbato G, Ikura M, Kay LE, Pastor RW, Bax AD (1992) *Biochemistry* **31**: 5269–78.
31 All programs and source codes are available from the authors upon request. E-mail IQOJJ01@PINAR1.CSIC.ES.
32 French AD, Brady JD (Eds) (1990) *Computer modelling of carbohydrate molecules*, ACS Symp. Ser., 430.
33 Homans SW (1990) *Biochemistry* **29**: 9110–18.
34 Siebert H-C, Reuter G, Schauer R, von der Lieth C-W, Dabrowski J (1992) *Biochemistry* **31**: 6962–6971.
35 Asensio JL, Martin-Pastor M, Jimenez-Barbero J (1995) *Int J Biol Macromol* **17**: 52–55.
36 Lemieux RU, Bock K, Delbaere LTJ, Koto S, Rao VS (1980) *Can J Chem* **58**: 631–53.
37 Rutherford TJ, Homans SW (1994) *Biochemistry* **33**: 9606–14.
38 Rutherford TJ, Neville DCA, Homans SW (1995) *Biochemistry* **34**: 14131–37.
39 Davis DG (1987) *J Am Chem Soc* **109**: 6962.
40 van Halbeek H, Poppe L (1992) *Magn Res Chem* **30**: S74–S86.
41 Leeflang BR, Kroon-Batenburg LMJ (1992) *J Biomol NMR* **2**: 495–518.
42 Gonzalez C, Rullman JAC, Boelens R, Kaptein R (1991) *J Magn Rason* **91**: 659–64.
43 Hajduk PJ, Horita DA, Lerner L (1993) *J Am Chem Soc* **115**: 9196–201.
44 Heatley F (1979) *Prog NMR Spectrosc* **13**: 47.
45 Wagner G (1993) *Curr Opin Struct Biol* **3**: 748–54.
46 a) Dais P (1994) *Carbohydr Res* **263**: 13–24. b) Poppe L, van Halbeek H, Acquotti D, Sonnino S (1994) *Biophys J* **66**: 1642–52. c) Engelsen SB, Herve du Penhoat C, Perez C (1995) *J Phys Chem* **99**: 13334–51.

Received 10 December 1996, revised and accepted 11 March 1997